Published in Composite Structures, doi:10.1016/j.compstruct.2015.09.062

Interaction of inter- and intralaminar damage in scaled quasi-static indentation tests: Part 2 - Numerical Simulation

XC. Sun*, M.R. Wisnom, S.R. Hallett

Advanced Composite Centre for Innovation and Science (ACCIS), University of Bristol, UK

Abstract

A numerical study, accompanied by the experimental data from Part 1 of this paper, provides a clear picture of the global damage behaviour and local response of four scaled Carbon Fibre Reinforced Polymer (CFRP) laminates under quasi-static transverse loading. Interface elements with a cohesive formulation are employed to model delamination, matrix cracks and their interaction. The predictive damage from different numerical simulations with different levels of detail is presented, and the validity is illustrated both qualitatively and quantitatively. Specifically the number of inserted potential intralaminar crack paths is varied from no cracks, through single, then double, to multiple cracks. It is shown that the models with the capability to simulate multiple matrix cracks best predict the key aspects of barely visible damage of composite laminate during quasi-static loading.

Key word: Interface elements; Impact damage; Finite Element Analysis (FEA); Fracture.

1. Introduction

Low-velocity impact of carbon-fibre reinforced laminated composites is one of the most critical loading conditions of aerospace structural components, because the mechanical properties of laminated composites are considerably weaker in the matrix-dominated directions. Two types of damage can be readily induced by such loading. They are delamination accompanied by matrix cracks, and back-face fibre breakage, which are called Barely Visible Impact Damage (BVID) in aerospace structural applications. This damage takes place inside the laminate and may not be easily inspected. Delaminations arising at the ply interfaces induced by transverse loading are apt to propagate during in-plane compressive loading, which is the one of the most common loading conditions for composite panels in today's aircraft primary structural components. The presence of delamination can lead to significant compressive strength reduction even without the presence of fibre breakage [1–8]. For this

reason, delamination and associated matrix cracks and their interaction are important mechanisms to be understood. The damage behaviour and damage mitigation of composites have thus been extensively studied and reviewed by both experimental and numerical approaches e.g. [9–14].

During an impact event, the laminate is subject to a complex loading condition, which causes compression at the top, tension at the bottom of the laminate, interlaminar shear stress inside the laminate and contact stress immediately under the impactor. Matrix cracking is recognised as an early damage mechanism before delamination, after which the stress is redistributed and causes stress concentrations at the locations where the matrix cracks intersect with resin-rich region at the adjacent ply interfaces. Because of the developed interlaminar shear stresses and the relatively weak mechanical properties of the matrix, delamination initiates from these matrix cracks. Since the matrix cracks are not able to penetrate adjacent plies with a different fibre orientation, the cracks tend to migrate from one ply to another by joining up via delaminations at the interfaces [15,16]. As the load increases, delamination growth at pre-existing locations and the occurrence of fibre breakage at surfaces result in the load-bearing capability of the laminate being completely disrupted. Therefore, non-critical damage mechanisms and coupling phenomena between matrix cracks and delamination before critical failure become extremely important for the study of both impact damage resistance and damage tolerance.

Owing to the strong demand for advanced, well-validated and robust numerical models for virtual testing in academia and industry, many efforts in studying, characterising and predicting the failure behaviours and damage mechanisms of laminated composite using the Finite Element Method (FEM) are reported in the literature. Numerical prediction of impact-induced damage can be generally categorised into continuum and discrete approaches. Both approaches usually rely on stress-based criteria for damage initiation and fracture mechanics for damage evolution. Material models for low-velocity impact damage prediction based on these two distinct approaches, Continuum Damage Mechanics (CDM) and Cohesive Zone Modelling (CZM), have been studied in the literature in recent years e.g. [17–20]. Lopes et al [21] used a three-dimensional progressive failure model to simulate intralaminar damage. A physically-based failure criterion [22] for damage initiation, and a mesh-independent evolution law adopted from Maimí [23] were employed. The delamination prediction was

modelled using CZM, and a good correlation with experimental results was obtained. Likewise, Shi et al [19] have used a stress-based damage model, for fibre failure and matrix cracks as well as taking nonlinear shear behaviour into account, and using cohesive elements at the interface of plies to model delamination, to predict damage in a cross-ply laminate under low-velocity impact. Enhancements to these models have been made recently by adding strips of interface elements at the intralaminar level for discretely simulating the matrix crack, and by this method the accuracy of predicted energy absorption and the splitting damage at the bottom ply was significantly improved [24].

The interest in implementing interface elements with CZM formulations into potential damage regions at the interlaminar level has increased, and the approach has become a standard feature in most commercial FEA software packages. The development and applications of deploying interface elements to predict discrete matrix-dominated failure has been reviewed by Wisnom [25]. Hallett et al [26] have showed the advantages of using interface elements with a CZM formulation to simulate intra and interlaminar damage in tension loaded scaled laminates with damage arising from the free edge, giving results that agreed with experimental observations very well. Aymerich et al [27], Lammerant and Verpoest [28], Moura and Gonçalves [29] and Zhang et al [30] all have simulated delamination and single matrix cracks at predefined locations using the CZM approach and studied the effect of matrix cracks and neighbouring fibre orientations on the behaviour of delamination propagation during low-velocity impact in cross-ply laminates. All delamination prediction was much improved compared to models without matrix cracks being modelled.

Bouvet et al [14] in contrast to these single crack models proposed a distinct formulation with an unique model architecture to take account of the effect of global matrix cracks on delamination of quasi-isotropic composite plates under impact loading. Each ply was meshed into small parallel strips along the fibre direction with one volumetric element. A zero length spring element was used to connect a group of four adjacent ply elements between parallel strips for simulating matrix cracking through a stress-based quadratic criterion. Delamination was also modelled in a similar manner using four individual spring elements to link the four nodes between each of the two consecutive plies. The

predicted individual delamination shape and overall response of the plate correlated with experimental observation extremely well.

CDM, on the other hand, has been considered as an accurate and less expensive modelling method than the CZM approach for complex structures. However, model size in CDM analysis is usually gradually increased as more plies are being modelled because continuum elements with a small characteristic length have to be placed over large potential damage regions to overcome such shortcomings as mesh-dependency and strain localisation [22]. This could lead to substantial increase in the computational cost if thin layers of cohesive elements between plies are globally deployed. Moreover, because the matrix-dominated damage (delaminations and matrix cracks) takes place at different locations, CDM may not allow intralaminar crack tips to capture the physical interaction with the interlaminar region.

Despite the large amount of information in the literature and numerous existing numerical studies, there has not yet been a systematic study on the level of detail with which the matrix cracking needs to be included in a model to achieve accurate results. Also there is a lack of highly detailed experimental data needed for correlation of such numerical studies across a sufficiently wide range of cases to validate the models. This has been addressed through a series of scaled indentation tests on specimens with different thicknesses and in-plane dimensions in Part 1 of this paper [31] and here an equivalently detailed study of the numerical modelling of such tests is presented. Cohesive elements were inserted in both inter and intralaminar levels systematically at potential damaged regions. Each ply was modelled as an orthotropic elastic material, and fibre failure has not been considered here since the priority of this study was to investigate the interaction between matrix cracks and delamination before the fibre failure initiation, which usually occurs after the formation of BVID. It has been noted that scaled tests provide a particularly rigorous case for model validation, especially when there is variation in the level of damage and failure response [32,33]. This approach has been followed in this study with both in-plane and full 3D scaling undertaken [33] to rigorously assess the models presented here.

The loading was undertaken at quasi-static rates in the experiments since it is advantageous, over low-velocity impact, to control the level of damage achieved. Many studies have shown the high degree of

equivalence between quasi-static indentation and low-velocity impact damage in laminated composites [34–39] and this was also confirmed here [31]. To distinguish the various impact events and static indentation processes, Olsson [39] has used a mass criterion to characterise different responses of composite plates under low-, intermediate- and high-velocity impact with small and large mass of impactor. This was shown to be an easy procedure to define the limit to approximate transverse impact response using quasi-static solutions such as that developed by Swanson [38]. Both authors suggested that a large-mass impactor, whose mass is at least ten times larger than the target plate and travels at a few m/s, and impacting a composite plate in the transverse direction is deemed to be a quasi-static process. The response of the substrate is a static deformation mode, and consequently the relation of the contact force and plate transverse displacement should match with that in the static indentation process. Aoki et al [34] and Nettles et al [40] have compared the damage behaviours of CFRP laminates under low-velocity impact and static indentation tests using various post damage inspection techniques. Regardless of minor dynamic and local effects, a high degree of equivalence between both test results in terms of load-displacement histories, damage mechanism and damage size was found. Numerical models in this study and experimental results in Part 1 of this paper based on static analysis are therefore considered to be reliable to model and replicate the damage behaviour of composite plates under large-mass, low-velocity impact.

2. Experiment

The experimental results used for validation of the numerical models are presented in detail in Part 1 of this paper [31], and pertinent information will not be repeated here except for the description of some key features of the specimens, damage mechanisms and test setup. Four types of scaled quasi-isotropic laminates were subjected to quasi-static indentation test, based on the ASTM standard for measuring the damage resistance of CFRP plates to drop-weight impact events [41]. During static indentation, several load drops and recoveries before complete penetration of the laminate by the indenter can be found in the load-displacement plot, and each load drop is reflected by the damage extent and mechanisms. The load level before the first significant load drop, referred to as the critical load or delamination threshold load, indicates the elastic limit of the laminate, which is one of the most

important factors to be considered in low-velocity impact damage studies. The load drop is caused by unstable delamination propagation at available interfacial regions [31]. In the experiment, ultrasonic C-scanning and X-ray Computed Tomography (CT) scanning were applied to thoroughly assess the damage extent in selected damaged laminates taken before and after the critical load to provide detailed information about the damage morphology and progression for model validation. The characteristics of these scaled specimens used in this study are listed in Table 1.

The relation between the four types of specimens covers both in-plane and thickness scaling. The In-plane scaled (Is) specimen has doubled in-plane dimensions compared to the Reference (Ref) specimen which serves as a baseline case, and a downscaled experimental apparatus including scaled supporting window and indenter size was also used in the Ref case. The baseline layup is $[45^o/0^o/90^o/-45^o]_{2S}$. Sublaminate scaling (Ss) and Ply-block scaling (Ps) specimen both have doubled in-plane dimensions compared to the Ref case, and a doubled overall thickness. In the Ss case the sublaminate group $[45^o/0^o/90^o/-45^o]$ is repeated four times in each half laminate. In the Ps case, the thickness is increased by blocking two plies with the same fibre orientation.

It has been found that blocking plies with the same fibre orientation leads to a drop in matrix cracking resistance, e.g. by Parvizi et al [42]. This is later referred to as the 'in-situ' effect [43], meaning the matrix-dominated in-plane strength of a ply is dependent on the number of plies clustered together, the orientation of adjacent plies and the ply position in the laminate . By varying the in-plane dimensions as well as using different thickness scaling methods, a variation in the matrix cracking and delamination has been achieved, and such scaled tests thus pose very challenging cases for validation of high fidelity numerical models [32,33].

3. Composite Laminate Model

3.1 Cohesive Formulation

By means of the CZM approach, the resin-rich regions between and within plies are modelled using cohesive element layers with finite thickness. The cohesive formulation developed by Hallett et al [44]

and Jiang et al [45] with 8552 toughened epoxy resin properties was adopted here and implemented into the non-linear explicit solver, LS-DYNA, via a user material subroutine. The entire cohesive formulation will not be elaborated here except for the description of the key equations.

A bilinear softening constitutive law which relates the traction and separation of the cohesive element in mixed mode fracture was applied, with the area under the bilinear curve being the critical Energy Release Rate (ERR) of the relevant fracture modes. A quadratic stress-based failure criterion presented in Eq.1 dictates the damage onset in mixed-mode loading, where σ_I and σ_I^* are the Mode I (opening) stress and strength, σ_{II} and σ_{II}^* are the Mode II resultant shear stress and strength (reflecting both Mode II and Mode III shearing). From this point onward the shear stress component will be denoted as σ_{II} in this manuscript, since at an element level the cohesive formulation can not determine the crack front orientation and thus not distinguish between Mode II and Mode III. Damage propagation is controlled by the fracture energy based mixed-mode power law shown in Eq.2.

$$\sqrt{\left(\frac{\sigma_I}{\sigma_I^*}\right)^2 + \left(\frac{\sigma_{II}}{\sigma_{II}^*}\right)^2} = 1 \qquad (1)$$

$$\left(\frac{G_I}{G_{IC}}\right)^{\alpha} + \left(\frac{G_{II}}{G_{IIC}}\right)^{\alpha} = 1 \qquad (2)$$

$$\begin{cases} \sigma_{II_n}^* = \sigma_{II}^* - \eta\sigma_I \\ G_{IIC_n} = G_{IIC}\left(\frac{\sigma_{II_n}^*}{\sigma_{II}^*}\right) \end{cases} \text{when } \sigma_I < 0 \qquad (3)$$

α is an empirical parameter ranging from 1.0 to 2.0 obtained by curve fitting from mixed-mode testing, G_{IC} and G_{IIC} are the critical ERRs of pure Mode I and II loading, and G_I and G_{II} are the pure mode components of ERR due to mixed-mode loading. It should be noted that this formulation takes account of the enhancement effect of through-thickness compression on shear behaviour, through which the shear strength and Mode II critical ERR are linearly increased by a material-dependent enhancement factor (η), in the presence of through-thickness compressive stress, as shown in Eq.3. $\sigma_{II_n}^*$ and G_{IIC_n} are the enhanced Mode II strength and critical ERR. This enhancement approach was adopted from Li et al [46] who studied the influence of compressive stress on damage initiation and evolution of Mode II failure using cut-ply and dropped-ply specimens. Three enhancement strategies were investigated and

the modelling results were validated with experimental results providing useful information in the current study. In a recent study Gan et al [47] have also experimentally and numerically characterised the effect of increased shear strength due to through-thickness compression with a modified double-notch shear test. It was therefore considered to be important to take the enhancement effect into account to accurately capture the Mode II behaviour in the case of out-of-plane loading such as impact. Cohesive parameters used in the analysis are consistent with those used in Part 1 and also given here in Table 2.

3.2 Laminate Model

8-noded cohesive elements (Type-19 in LS-DYNA) with finite thickness were assigned to represent the behaviour of the resin-rich regions. These were introduced to the meso-scale laminate models (see Figure 1(a)) at intra and interlaminar locations to predict the matrix crack and delamination simultaneously during the virtual testing. Fibre failure and other damage modes were not taken into consideration in this study. A single layer of reduced integration 8-noded brick elements (Type-1 in LS-DYNA) with elastic orthotropic material properties (see Table 2) was used to model each single ply. Different numbers of strips of intralaminar elements were vertically inserted at predefined region crossing the centre of each ply and parallel to the fibre direction to physically capture the potential matrix cracking (split) paths. The intralaminar elements near the bottom ply were to simulate the transverse (bending) cracks due to tension developed during plate deflection, while intralaminar elements embedded elsewhere were to model the shear cracks caused by through-thickness shear stresses. Thin layers of interlaminar elements were inserted at each interface region between plies of dissimilar fibre orientation to predict delaminations. The total numbers of representative matrix cracks modelled and their spacing was motivated by the X-ray CT-scan observations. By altering the numbers of intralaminar splits from 0 to 6, allowing the occurrence of matrix cracks at a predefined region of interest, the optimal crack density, damage behaviour, damage interaction, plate overall response and delamination shape of the four types of scaled laminates during indentation virtual tests were evaluated.

Four types of models with different numbers of potential splits were proposed for each case shown in Table 1, termed as 0-split, 1-split, 2-splits and 6-splits. The nodal connectivity and architecture of these laminate models are shown in Figure 2. All nodes were merged in the 0-split and 1-split models, and

their meshes were identical except that a single strip of cohesive elements was placed inside the 1-split model in each ply without interrupting the nodal connectivity. Due to the complex and different mesh schemes in plies and interfaces, segment based tied constraints were used to permanently bond parts with different mesh densities in the 2-splits and 6-splits models. The blocked-ply Ps case has a different effective ply thickness (h_f), which was set to 0.25mm instead of 0.125 mm being used in the rest of the cases. The thickness of the cohesive elements, h_c, was 0.005mm for normal-ply laminates (Ref, Is and Ss) and 0.01 for blocked-ply laminate Ps, which is sufficiently small so that the intralaminar element layers would not significantly alter the in-plane and out-of-plane properties of each ply and the thickness ratio between a single ply and a intralaminar layer was consistent for all cases. With the addition of the interlaminar layers the overall thickness would be marginally increased. The overall thickness of each laminate model was then scaled to be equal to that of actual laminate measured in the experiment. The no split model (0-split) does not have any intralaminar elements. The single split model (1-split) has a single centre split in each ply, under the point of loading indicated in Figure 3(a). The double split model (2-splits) has two parallel splits in each ply either side of the loading point, and the multiple split model (6-splits) has six splits evenly distributed in a wider band under the loading point (see Figure 1(b) and Figure 3(c)). The split spacing shown in Figure 1(b) was based on the X-ray CT-scans of damage specimens. Figure 3(a) & (c) show the ply mesh and the location of intralaminar element strips of each case. Because it is necessary to have a sufficient number of elements in the softening region along each crack propagation direction to obtain accurate analysis using interface elements, the cohesive element length along the crack path was calculated by the procedure from Harper and Hallett [48]. Cohesive elements with an optimal length of 0.2 mm were then used in the Region of Interest (ROI) shown in Figure 3(b) and (d), its length is gradually increased away from the ROI to reduce computational cost. The dimension of ROIs was predefined according to the maximum projected delamination size observed for all cases in the experiment. Although the mesh of these models were not the same because of the size of the plate and different number of splits being included in the model, an identical cohesive element size in the ROIs was used in all models. Selected models with halved cohesive element length (0.1 mm) and doubled mesh density in the plies were tested for a mesh sensitivity study. No

discrepancies in overall response were found, and less than 2% difference in interlaminar shear stress history and detailed damage prediction was achieved compared to the proposed mesh schemes.

Solid elements with rigid material properties were used in modelling the supporting windows and the indenters. A prescribed displacement rate was given to the rigid indenters to simulate the indentation process. A penalty based contact formulation was used between the rigid parts and the laminate, and a static friction coefficient of 0.3 was assigned. In order to minimise the computational cost whilst retaining accuracy of the results, the densities of all materials were scaled up by three orders of magnitude to increase the minimum time step size, and no significant dynamic effects were found during quasi-static loading. Hourglass control (Type-6 in LS-DYNA) was defined for all reduced-integration elements to supress zero strain energy distortion modes, and hourglass energy was compared to the system internal energy at the end of each analysis to ensure it remained negligible. Reduced integration solid elements (LS-DYNA Type-1) for orthotropic plies were considered to be sufficient for avoiding transverse shear locking effects [49]. For accurate analysis, a thermal load of -160^{o}C was incorporated into each simulation prior to the indentation loading to model the 'cooling down' of the laminate after the curing process and accounts for thermal residual stresses.

4. Results and Discussions

4.1 Overall Plate Response

The performance of the numerical models was thoroughly assessed by comparison with the experimental load-displacement curves and damage morphology from damage inspection via X-ray CT-scan. To validate the overall response of the composite plate models and to evaluate the effectiveness of the four modelling approaches with increasing number of splits, a set of comparison is presented in Figure 4. A good correlation of initial stiffness before the first load drop can be seen for each case and each modelling approach. A slightly lower stiffness can be noticed in most 1-split models compared to 0-split models. This is because the splits near the bottom of the plate open in the early stages of indentation due to tension, leading to a local stiffness degradation in 1-split models. As previously described, different techniques were used in 0/1-split and 2/6-splits laminate models to introduce

delamination interface elements. All nodes were coincident and merged in the 0/1-split models, while multiple tied contacts (28 for 16-plies laminates and 60 for 32-plies laminate) had to be defined in the 2/6-splits models in order to connect the plies and interlaminar layers with different meshes. The stiffness of the 2-splits and 6-splits models increased slightly from that of the 0/1-split models in contrast to the expected effect of reduced stiffness with increasing number of splits. This was believed to be caused by the introduction of the tied contact definition (*TIE_SURFACE_TO_SURFACE). To verify this, two trial models were built. The first model was based on the Ref 0-split model but with tied contact defined between the interfaces and plies. Its stiffness was slightly higher than the Ref 0-split model and similar to Ref 2/6-splits models. The other model was based on Ref-6 splits meshes but without any splits, similar initial elastic stiffness was observed compared to Ref 2/6-splits model. Other trial models were performed before the indentation simulations to evaluate the best contact definitions to use, with the least effect on the overall compliance of the laminate. Nevertheless, a slight contribution from the multiple constraints to overall stiffness in these complex laminate configurations seems inevitable, but its effect is small compared to the stiffness changes due to the evolution of damage. Results within a defined modelling technique (i.e. 0/1 or 2/6 splits) are consistent with expectations; that an increasing number of splits reduces the compliance as local damage develops, before the first load drop. The load levels at which the first major drop occurs (critical load for delamination propagation) in the 2-splits and 6-splits models of each case generally agrees well with the experimental results. The critical load in the 1-split models are lower than those of 0-split models in most cases. In general, a more accurate prediction of the critical load is achieved with an increasing number of splits. Figure 5 collectively compares the critical load between the experiments and virtual tests. It is clear to see that the predicted critical load approaches the test results as the number of virtual splits increases, and the prediction given by 6-splits models achieves a less than 5% difference compared to the test results in all cases. It is noted that one of the largest discrepancies comes from the 0-split model for the Is case, and the prediction is much improved in models with split(s). This is because the Is plate has a lower thickness-to-width ratio and consequently lower bending rigidity [10]. The back-face tension therefore contributes more to the loading response, with the virtual split(s) predicting early damage initiation and reducing the overshoot in critical load prediction of the 0-split Is model. It also can be

seen that models with a single virtual split may not be sufficient to correlate the behaviour of the actual plate at the moment of load drop, particularly as the number of plies increases such as in the Ps and Ss cases. It is difficult to determine a general trend between the number of splits in the models and the levels of scaling. This is because the delamination propagation is primarily driven by the interlaminar stress state and the first damaged interface(s), which is the result of a complex interaction between a number of factors, and can only partially be attributed to the number of splits in the model. The number of splits as a driving factor cannot therefore be taken in isolation. For the smallest 'Ref' case the load does increase consistently with the number of splits, but this trend is not repeated for the rest of the scaled laminates. As the laminate in-plane size and thickness are scaled, these too have an effect on the interlaminar stress state and the way that delaminations join up once propagating. Thus it is not only that there are not consistent trends in the level of load drop across the scaled specimens for increasing numbers of splits, but there is also variation in the damage pattern associated with this load drop, as discussed in section 4.2.

4.2 Overall Damage Prediction

As well as the load-displacement curves and effect of damage modelling on the critical load, it is also informative to look at the various damage patterns predicted and their correlation to test (see Figure 6). At the bottom of Figure 6, a top view of the delamination and matrix cracks of each test case from [31] taken after the critical load drop is shown. Delamination occurring at interfaces with the same relative orientations are coloured according to the given figure legend. These images allow readers to see the complete picture of the delamination patterns which have been segmented through post-processing of CT images. The delamination and the back-face split size can be compared with the help of a scale bar. Due to the compressive stress caused by the indenter during indentation and the highly localised deformation of the top ply, there is a 'delamination-free' zone at the centre of the damage and delaminations are supressed in all cases at the top [$45^o/0^o$] interface. Figure 7 quantitatively shows the number of predicted delaminated interfaces from the models and the projected delamination area against these experimental results. In Figure 7(a), it can be seen that 0-split models for all cases have poor correlation compared to other modelling approaches; especially for Is and Ps cases where the difference

from test results is up to 60%. As the split numbers increase towards 6, the number of damaged interfaces nearly doubles for these two cases. In contrast to the 0-split, the 6-splits models give very good delamination distribution predictions compared to the test results. The strong influence of virtual splits can also be seen by comparing the projected delamination area shown in Figure 7(b). A large difference in delamination area can be found in 0-split models for Ps and Ss, which is caused by unstable delamination growth at interfaces near the bottom surface of the plate, which dominates the overall projected area. The inclusion of more than one split significantly improves the prediction across all four cases. Regarding the overall damage size and distribution, all models with 6 splits are able to provide very good correlation with the experimental results.

4.3 Detailed Delamination and Matrix Crack Comparison

In order to quantitatively validate the numerical prediction to a high level of detail, the individual delamination shape and size at each interface was obtained from the post-processed X-ray CT data and then compared with the model predictions. Only a sub-set of the results are presented here for brevity. Since the models with 6 splits achieved the best correlation at the overall level as presented in the previous section, only this model is compared here in more detailed level. The left diagram in Figure 8 shows the X-ray images of each individual delamination of the Ps case after the first load drop, and the prediction from the 6-splits model is shown on the right. The best prediction is found at interfaces with a 90^o angle difference between adjacent plies (delamination at [+/-45^o] and [0^o/90^o] interfaces) shown by green and cyan. Delamination initiates at a pair of transverse shear cracks and propagates along the fibre direction of the lower neighbouring ply. The damage interaction was also well captured. The pair of fan shaped predicted delaminations can be found in interfaces with plies with a 45° difference, these delaminations are enclosed by pairs of matrix cracks in the adjacent plies, which implies that matrix cracks play an important role in the extent of damage formation. Although the numerical prediction of these gives a slightly greater delamination area, particularly in the region between the pairs of matrix cracks, the overall predicted extent of delamination is very similar to the test. The largest delamination observed is at the fourth 90^o interface which coincides with the numerical prediction. In general, the

shape and size of each delamination prediction by the 6-splits model agrees very well with the experimental results.

Comparison of the projected delamination area is often used for model validation in the literature. The overall size of it may be overshadowed by a single or few delaminations, usually at 90^o angle difference interfaces in the lower section of the laminate. In this study it has also been possible to compare the total delamination area for each model configuration for further validation due to the high fidelity of the experimental data and models available. Figure 9 shows the bar chart of total delamination measured from each separate interface and numerical prediction for the four laminate configurations and four modelling methods. The total delamination area can be treated as an indication for the amount of energy being released after the first significant load drop. The largest difference between prediction and observation is found in the 0-split and 1-split models in the Ss case, which is similar to the results in Figure 7 (b). Considering the prediction of the number of delaminated interfaces and the projected delamination area of each model (see Figure 7), it shows that the predicted delaminations in Ss 0-split and 1-split models were not fully developed, and the number of delaminated interfaces was less than observed due to the lack of fidelity in intralaminar damage. Consequently, the projected and total delamination area predicted in these models has less agreement with the experimental observations. Without matrix cracks being included in the Ps 0-split model, it experienced a rather unstable delamination propagation at only half the number of the observed delaminated interfaces, causing a large projected delamination area but it still gives a relatively good prediction in total delamination area. It can thus be seen that the delamination formation is profoundly influenced by the number of cracks. For the zero split case, delaminations can not join up at all between interfaces. For the single split case the crack is placed directly beneath the indenter and so is not subject to transverse shear stresses that are the main driving force for crack formation. The experimental evidence in Part 1 shows that cracks do not form directly under the indenter but either side of it instead. Thus the 2-split model is more representative and has a better agreement with experiment in terms of projected and total delamination area and is close to the 6-split model result.

It is also considered to be important to validate the predictions of the development and extent of characteristic matrix cracks which, as the first failure mechanism, define the elastic limit of the laminates under point loading. This is also done only for the most accurate 6-splits model. In order to study the interaction between delaminations and matrix cracking, the model should be in a good agreement with experimental observation for both damage mechanisms. Figure 10 presents the matrix cracks for the Ps case in the prediction and experimental results from the CT-scan at selected locations. This shows multiple matrix cracks located in neighbouring plies, which are deemed to interact with the delaminations at the corresponding interfaces. It can be seen that the cracking patterns have a close match to the overall shape of delamination, similar to that shown in Figure 8. Because of the stochastic nature of the occurrence of actual matrix cracks, it may not be possible to explicitly model the exact number and location of the multiple micro-cracks, however the longest cracks that play an important role in delamination are the most important to be studied. The length of the longest matrix cracks that interact with the direction of delamination growth should be captured by the model. It can be remarked that, regarding only the length scale of the simulated matrix cracks, the FE model results provide good prediction of the extent of characteristic matrix cracks. A more refined pattern of pre-inserted potential characteristic cracks would be required to capture the full details of the cracking pattern.

4.4 Damage Evolution and Delamination Sequence

Experimental observation shows the first damage mechanism before the first significant load drop is transverse cracks near the bottom of laminates due to tension and shear cracks near the plate mid-plane due to interlaminar shear stresses in the Ref and the Is cases [31]. However, delamination crack propagation is much more unstable than splits, and questions like the location of the first delamination or the direction of delamination propagation during low-velocity impact can never be explicitly answered from the experiments. It is reasonable to assume that if the proposed high fidelity models are able to accurately predict the final damage extent in high level of detail, the simulation of the evolution and sequence of damage development is also valid, which can give valuable insight into the failure mechanisms.

An ultra-fine sequence of results output was generated by the simulation near the critical load drop in order to illustrate the predicted damage evolution and the delamination sequence. Taking the 6-splits model of the Ref case as an example here. Damage evolution is presented by snapshots of the overall damage pattern, taken at six time points on the load-displacement curve shown in Figure 11(a). Point A and B are before the first load drop. Points C to F are taken immediately after the first load drop. Cut-section views and overall damage extent are presented in Figure 11(b). Corresponding indenter displacement (ω_i) of each time point is shown on the cross-section images. At point A, a back-face transverse crack as the initial damage mechanism is formed at a very early stage, after which the transverse cracks propagate and migrate toward the upper plies as the load increases to point B. After the load reaches the critical level shown as point C, the first appearance of delamination occurs at the two adjacent interfaces [-45^o /90^o] above and below the [-45$^o{}_2$] ply at the symmetry plane, where the interlaminar stresses are high and not influenced by the through-thickness compression, and are joined by a matrix crack in the [-45$^o{}_2$] ply. The delamination then migrates to the [0^o/45^o] interface above via matrix cracks in the 0^o and 90^o plies at point D, after which delamination propagates from the mid-plane towards the lower interface [0^o/45^o] shown as point E. Then, it substantially extends in both the upper and lower directions simultaneously (point F). After the first load drop and load recovery, delaminations occur at every possible interface and then further develop with increasing load. The location of the first appearance of delaminations predicted by the highest level of fidelity, 6-splits model, is in good agreement with the assumptions made in analytical predictions for the delamination threshold in static and low-velocity impact [50].

In general, the predicted damage evolution coincides with the experimental observation. However, the 6-splits model was not able to capture the transverse shear cracks before the load drop, at the mid-plane which were observed in the experiment [31], because such shear cracks occur at an inclined fracture angle [51] and the inserted intralaminar elements were placed vertically to the plies for simplicity. For this shear loading, the splits in the 6-splits models would not have the correct orientation and stress components and thus would not fail and open accurately. However, since the 6-splits models give a reasonable prediction of maximum crack length and detailed delaminations after the load drop, the

correlation with shear cracks before the load drop may not be necessary. From point F in Figure 11(b) after the predicted delamination is fully established, it is clear to see that the predicted matrix cracks are in a 'staircase' pattern, interconnecting neighbouring delaminations. Moreover, the delamination structure shows the well-documented 'pine tree' shape through the thickness direction of the laminate. According to the experimental observations and the predicted damage evolution, it can be said that the 6-splits models were able to simulate the damage extent as well as the damage sequence.

4.5 Scaling

Simple analysis provides basic and quick estimation of fundamental characteristics such as plate global response and critical load for delamination propagation derived from plate theory [51] and linear elastic fracture mechanics [52]. The results from experiments and analytical solutions, which were presented in Part 1, can be compared to the more detailed numerical modelling presented here. This allows an exploration of the key driving parameters for the scaling effects and to quantitatively evaluate the fidelity of both predictive methods.

Table 3 shows the comparison of critical loads of each case between test data and both analytical and numerical predictions, using the most accurate 6-splits models. Generally, the numerical results give a more accurate prediction than analytical methods for the critical load, especially for the Ref and Ps cases, with less than 12% error. This shows some limitation of the analytical solutions caused for example by the exclusion of intralaminar failure and multiple interface delamination.

The Ref and Ps cases, are a true fully scaled pair and follow the 'similitude law' [53] in all senses including in-plane, ply thickness, overall thickness as well as the test apparatus. The flexural stiffness of Ref and Ps laminates follow the 'similitude law' up to the onset of damage after which strong nonlinearity is involved [31]. There is good agreement between the global response and damage pattern in both experimental observations and numerical models, as shown in Figure 4 and Figure 6. Critical load predictions from both the analytical and numerical (6-splits) solutions are slightly overestimated for both Ref and Ps cases (see Table 3), which are reflected in the overestimation of projected delamination area (see Figure 7(b)).

With the scaling methods for scaling the delamination size after the critical load shown in Part 1 for the true scaled pair the Ref and the Ps cases, numerical results match the scaling factor between them well, as can be seen in the following expression:

$$\frac{a_{Ps}}{a_{Ref}} = \begin{matrix} 2.00 & \textit{Theoretical} \\ 2.05 & \textit{Experimental} \\ 2.02 & \textit{Numerical} \end{matrix}$$

where a is the radius of initial projected delamination after the first load drop. The numerical result here was from 6-splits models of the Ref and Ps case, the delamination radius was calculated from the projected delamination area (as it was for the experimental result). The consistent result between that derived from simplified fracture energy based initiation criteria [54], experimental and numerical (6-splits models), further confirms that the initial damage scaling is based on the geometric parameters of the laminate. The assumptions made in deriving the theoretical solution in Part 1 together with the discussion of delamination sequence in the previous section imply that the interlaminar shear stress near the plate mid-plane, the material fracture toughness and the geometric nonlinearity developed accounting for damage in the laminate all play key roles in the delamination formation. This information can help to develop scaling laws that have the capability for scaling damage size, post-damage response and can provide better understanding of scaling effects in static indentation as well as in low-velocity impact events.

The Is laminate, compared to the rest of the cases, has a lower thickness-to-width (unsupported width of the laminate) ratio, which is studied as an important parameter for plate response in the literature [35]. Therefore, this laminate seems to be a special case in that the membrane-stiffening effect or geometric nonlinearity [54,55] plays an important role not only in the early elastic region before the load drop but also in counteracting global stiffness degradation due to delamination. This has been shown in both simulation and experimental results in Figure 4(c & d).

For sublaminate level scaling (the Ps and Ss cases), a higher critical load was observed for the standard-ply thickness laminates of Ss compared to the thick-ply laminates of Ps both experimentally and

numerically. It is therefore of some interest to compare the laminate behaviours and stress states leading up to the failure. Figure 12 shows a force-displacement curve comparison of the Ps and the Ss 6-splits models; the point of the transverse crack initiation for each case is marked on the curves as reference points. This higher damage resistance to transverse loading in the Ss laminate is the result of the increased resistance to matrix cracking for thinner plies, sometime described as the 'in-situ' effect. The force-displacement curves and the damage extent after the load drop of both cases agree with the experimental results very well (see Figure 4–7), which allows a comparison to be made between the highest fidelity models for their structural response and interfacial stress state at four different displacement levels before the occurrence load drop of the Ps case (shown in Figure 12). The first and second comparison points ($\delta = 0.25$ and $0.55\ mm$) correspond to the moments of the first appearance of transverse crack in the Ps and Ss cases, respectively. The third one is at $\delta = 1.0\ mm$ and is located between the second and the last comparison points. The last point ($\delta = 1.40\ mm$) is at the point just before the load drop in the Ps 6-splits model. Figure 13 (a) & (b) respectively shows the top and the bottom ply out-of-plane deflection profiles at the centre of the laminate model along the longitudinal direction (x axis) at the previously defined four comparison points in the Ps and Ss 6-splits models as shown in Figure 12. Due to the similar global flexural stiffness of the Ps and the Ss 6-splits models, their compliances, up to the load drop in the Ps 6-splits model, are extremely similar, however, the deflection profiles are slightly different after the onset of matrix cracking. As the indenter displacement (δ) increases ($\delta > 0.25\ mm$), the top (z = 2 mm) and bottom (z = -2 mm) deflections along x-axis, away from the centre point, in the Ps model are slightly larger than for the Ss model for given longitudinal locations. However the difference in deflection at the same longitudinal location is similar between the two cases. Thus, the overall deflection profile of the Ss is more localised than the Ps model. The same behaviours were also captured by comparing the x-axis deflections at difference indenter displacement levels between the Ps and Ss 0-split models. In other words, the thin-ply laminate Ss 6-splits model behaves as the same as the Ps case regarding to global behaviour, but it appears to be more flexible at the ply level, resulting in a relatively stronger ply-level nonlinearity compared to the Ps case as the deflection increases. Given that the predicted critical load in the Ss model is noticeably higher than that in the Ps case, the discrepancies in the surface deflection profile are believed to be the result

of the different ply thickness, which in turn leads to the variations in internal stress/strain states at each individual ply and interface. Figure 13 suggests that the overall interlaminar stresses of the Ss 6-splits model is lower than the Ps 6-splits model at each corresponding through-thickness and in-plane location. To verify this, Figure 14 shows the interlaminar shear stress state in a single interface adjacent to the mid-plane, the most vulnerable interface to failure, at the same displacement levels in the Ps and Ss 6-splits models. This interface is directly below the mid-plane blocked -45^{o} plies and adjacent to the [90$^{o}_{(2)}$] ply. The interlaminar shear stress shown in Figure 14 is the Mode II stress, σ_{II}, defined in Eq.1 in the interlaminar cohesive elements. The comparison is made at the moment just before the load drop in Ps 6-splits model where $\delta = 1.40\ mm$. It can be seen that the peak interlaminar shear stress in Ss is generally less than that in the Ps 6-splits model by up to about 14% near the centre of the plate, and the energy release rate can also be expected to be lower. Hence, the interlaminar shear stress in the Ps case seems to develop more quickly than that in the Ss case under the same indenter displacement. This leads to the critical energy release rate being reached earlier in the Ps case and consequently provoking delamination propagation and the critical load drop. The local stress oscillations shown in Figure 14 are caused by the interaction between intra- and interlaminar cohesive elements. The asymmetric stress distribution with respect to the centre where y = 0 mm is due to the axial asymmetric splits in the bottom -45^{o} ply interacting with the interlaminar interface elements and affecting the stress distribution. These modelling techniques that consider the intra-laminar splitting, inter-laminar delamination and their interactions during failure have also been implemented into other virtual testing environments with various laminate configurations. For example open hole tensile tests are studied in [57], and failure modes, trends and strengths in sublaminate and ply level scaled laminates, similar to the Ps and Ss cases here, were successfully captured by this current approach. Thus overall there is a high degree of confidence in the modelling technique itself and together with the highly-detailed experimental observations presented in Part 1, the modelling results of the Ps and Ss 6-splits are able to provide insights into the effects of ply blocking of laminates under transverse loading. From the differences in deflection profiles in Figure 13 (a) & (b), the interlaminar stress states at the mid-plane shown in Figure 14 and the critical load predictions in Figure 12 between the Ps and Ss 6-splits models, a possible explanation for the effect of ply-thickness scaling on delamination propagation has been given.

5. Conclusion

Static indentation tests on composite laminates were modelled to simulate not only the damage extent but also the damage evolution and delamination sequence typical of that induced by low-velocity impact. Four numerical models with different matrix cracking density were proposed, and the effectiveness and correlation with experimental results were investigated thoroughly via load curves and X-ray images. The four modelling strategies are generally able to give good predictions of overall delamination size compared to the test data. The level of correlation in terms of delamination size, individual shape, and matrix crack pattern increases with the number of matrix cracks embedded in the model. Numerical models with multiple splits embedded are able to provide far more accurate and detailed prediction than analytical solution based on circular thin plate and other models with zero, single and double splits.

More importantly, information on the damage evolution and the sequence of delamination propagation was illustrated by using the 6-splits model. For thin laminated composite plate under transverse point loading, the high fidelity numerical model captured the first appearance of delaminations that are located at interfaces above and below the mid-plane of the laminate. Together with the experimental observation showing that the shear cracks in the plies near the mid-plane occur at a load level lower than the threshold load for delamination growth, the first delaminations were considered to be triggered by these shear cracks along with the high interlaminar shear stress and then take place at available interfaces near the mid-plane of the laminate. This is considered to be valuable for studying impact damage mechanisms, impact damage resistance and damage mitigation strategies.

Models with few or no discrete matrix crack elements are not able to accurately predict the delamination at every interface that occurs in the tests, but are able to provide basic plate response before the first load drop occurs, and some of them even give good correlation with test results after the load drop. It was found that the plate responses have a close relation to the ratio of ply thickness to characteristic length of the laminate. Also the ply thickness has an effect on the interlaminar shear stress distribution and the critical load for delamination propagation for laminates having the same overall thickness. Furthermore, the predictions for initial damage size scaling of fully scaled laminates (the Ref and Ps cases) were compared theoretically, experimentally and numerically. It was suggested that, for a given

stacking sequence and boundary condition, the scaling of the initial projected delamination sizes of fully-scaled laminates is closely related to their geometric parameters. Comparing the detailed ply level deflection profiles between ply level scaling pair provided by the Ps and the Ss 6-splits models, the ply thickness plays a role in the interlaminar stress level and in turn influences the critical load level and the delamination propagation.

This study was undertaken to better understand the interaction of matrix cracks and delamination and to investigate the level of detail of the matrix cracks that needs to be included in the model to achieve highly accurate predictions. In order to complete the numerical modelling investigation on composite damage during transverse loading, based on the confidence in the current static indentation modelling, low-velocity impact simulations will be important future works. This may require simulation of other damage modes and material characteristics influencing the impact behaviours, such as permanent indentation, fibre failure, nonlinear-shear and their interactions. Additionally, to complete the modelling strategy for damage tolerance analysis in the next step, the proposed models should not only predict damage from the indentation/impact loading but also from the subsequent in-plane compression i.e. Compression after impact (CAI). The accuracy of the predicted damage extent and distribution from low-velocity impact and quasi-static indentation will significantly affect the results of CAI modelling, and will also be the subject of future work.

6. References

[1] Ishikawa T, Hara E, Matsushima M. Examination of compression after impact (CAI) test method and relationships with open hole compression (OHC). ICCM13 proceedings, 2013, p. 1421.

[2] Ishikawa T, Sugimoto S, Matsushima M, Hayashi Y. Some experimental findings in compression-after-impact (CAI) tests of CF/PEEK (APC-2) and conventional CF/epoxy flat plates. Composites Science and Technology 1995;55:349–63.

[3] Ghelli D, Minak G. Low velocity impact and compression after impact tests on thin carbon/epoxy laminates. Composites Part B: Engineering 2011;42:2067–79.

[4] Cairns DS, Minguet PJ, Abdailah G. Theoretical and experimental response of composite laminates with delaminations loaded in compression. Composite Structure 1994;27:0–6.

[5] Soutis C, Curtis P. Prediction of the post-impact compressive strength of CFRP laminated composites. Composites Science and Technology 1996;3538:677–84.

[6] Baker A, Jones R, Callinan R. Damage tolerance of graphite/epoxy composites. Composite Structures 1985;4:15–44.

[7] Hawyes VJ, Curtis PT, Soutis C. Effect of impact damage on the compressive response of composite laminates. Composites - Part A: Applied Science and Manufacturing 2001;32:1263–70.

[8] Lee J, Soutis C. A study on the compressive strength of thick carbon fibre–epoxy laminates. Composites Science and Technology 2007;67:2015–26.

[9] Harding MM, Ruiz C. The Mechanical Behaviour of Composite Materials under Impact Loading. Key Engineering Materials 1998;141-143:403–26.

[10] Abrate S. Impact on composite structures. Cambridge University Press; 2005.

[11] Davies GAO, Zhang X. Impact damage prediction in carbon composite structures. International Journal of Impact Engineering 1995;16:149–70.

[12] Cantwell W, Morton J. Comparison of the low and high velocity impact response of CFRP. Composites 1989;20:545–51.

[13] Aymerich F, Dore F, Priolo P. Simulation of multiple delaminations in impacted cross-ply laminates using a finite element model based on cohesive interface elements. Composites Science and Technology 2009;69:1699–709.

[14] Bouvet C, Castanié B, Bizeul M, Barrau J-J. Low velocity impact modelling in laminate composite panels with discrete interface elements. International Journal of Solids and Structures 2009;46:2809–21.

[15] Chang F. A Model for Predicting Damage in Graphite/Epoxy Laminated Composites Resulting from Low-Velocity Point Impact. Journal of Composite Materials 1992;26:2134–69.

[16] Sridharan S. Delamination behaviour of composites. 1st ed. Woodhead Publishing; 2008.

[17] Donadon MV, Iannucci L, Falzon BG, Hodgkinson JM, de Almeida SFM. A progressive failure model for composite laminates subjected to low velocity impact damage. Computers & Structures 2008;86:1232–52.

[18] Kim E-H, Rim M-S, Lee I, Hwang T-K. Composite damage model based on continuum damage mechanics and low velocity impact analysis of composite plates. Composite Structures 2013;95:123–34.

[19] Shi Y, Swait T, Soutis C. Modelling damage evolution in composite laminates subjected to low velocity impact. Composite Structures 2012;94:2902–13.

[20] González EV, Maimí P, Camanho PP, Turon A, Mayugo J a. Simulation of drop-weight impact and compression after impact tests on composite laminates. Composite Structures 2012;94:3364–78.

[21] Lopes CS, Camanho PP, Gürdal Z, Maimí P, González EV. Low-velocity impact damage on dispersed stacking sequence laminates. Part II: Numerical simulations. Composites Science and Technology 2009;69:937–47.

[22] Pinho ST, Iannucci L, Robinson P. Physically based failure models and criteria for laminated fibre-reinforced composites with emphasis on fibre kinking. Part II: FE implementation. Composites Part A: Applied Science and Manufacturing 2006;37:766–77.

[23] Maimí P, Camanho PP, Mayugo J a., Dávila CG. A continuum damage model for composite laminates: Part II – Computational implementation and validation. Mechanics of Materials 2007;39:909–19.

[24] Shi Y, Pinna C, Soutis C. Modelling impact damage in composite laminates: A simulation of intra- and inter-laminar cracking. Composite Structures 2014;114:10–9.

[25] Wisnom MR. Modelling discrete failures in composites with interface elements. Composites Part A: Applied Science and Manufacturing 2010;41:795–805.

[26] Hallett SR, Jiang W-G, Khan B, Wisnom MR. Modelling the interaction between matrix cracks and delamination damage in scaled quasi-isotropic specimens. Composites Science and Technology 2008;68:80–9.

[27] Aymerich F, Dore F, Priolo P. Prediction of impact-induced delamination in cross-ply composite laminates using cohesive interface elements. Composites Science and Technology 2008;68:2383–90.

[28] Lammerant L. Modelling of the interaction between matrix cracks and delaminations during impact of composite plates. Composites Science and Technology 1996;56:1171–8.

[29] De Moura MFS., Gonçalves JP. Modelling the interaction between matrix cracking and delamination in carbon–epoxy laminates under low velocity impact. Composites Science and Technology 2004;64:1021–7.

[30] Zhang Y, Zhu P, Lai X. Finite element analysis of low-velocity impact damage in composite laminated plates. Materials & Design 2006;27:513–9.

[31] Abisset E, Daghia F, Sun X, Wisnom MR, Hallett SR. Interaction of inter- and intralaminar damage in scaled quasi-static indentation tests: Part 1 - Experiments. Submitted to Composite Structures 2015.

[32] Hallett SR, Green BG, Jiang WG, Wisnom MR. An experimental and numerical investigation into the damage mechanisms in notched composites. Composites Part A: Applied Science and Manufacturing 2009;40:613–24.

[33] Abisset E, Daghia F, Ladevèze P. On the validation of a damage mesomodel for laminated composites by means of open-hole tensile tests on quasi-isotropic laminates. Composites Part A: Applied Science and Manufacturing 2011;42:1515–24.

[34] Aoki Y, Suemasu H, Ishikawa T. Damage propagation in CFRP laminates subjected to low velocity impact and static indentation. Advanced Composite Materials 2007;16:45–61.

[35] Nettles A, Douglas M. A comparison of quasi-static indentation to low-velocity impact. NASA Technical Report 2000;NASA/TP-2000-210481,2000.

[36] Lee SM, Zahuta P, Corpornrioti C. Instrumented impact and static indentation of composites. Journal of Composite Materials 1991:204.

[37] Stout MG, Koss D a., Liu C, Idasetima J. Damage development in carbon/epoxy laminates under quasi-static and dynamic loading. Composites Science and Technology 1999;59:2339–50.

[38] Swanson SR. Limits of quasi-static solutions in impact of composite structures. Composites Engineering 1992;2:261–7.

[39] Olsson R. Mass criterion for wave controlled impact response of composite plates. Composites Part A: Applied Science and Manufacturing 2000;31:879–87.

[40] Nettles A, Douglas M, Estes E. Scaling effects in carbon/epoxy laminates under transverse quasi-static loading. NASA Technical Report,NASA/TP-1999-209103,1999.

[41] ASTM standard D7136 / D7136M. Standard Test Method for Measuring the Damage Resistance of a Fiber-Reinforced Polymer Matrix Composite to a Drop-Weight Impact Event 2003.

[42] Parvizi A, Garrett KW, Bailey JE. Constrained cracking in glass fibre-reinforced epoxy cross-ply laminates. Journal of Materials Science 1978;13:195–201.

[43] Davila C, Camanho P. Physically based failure criteria for transverse matrix cracking. 9th Portuguese conference on fracture, 2004, p. 1–8.

[44] Hallett SR, Wisnom MR. Numerical Investigation of Progressive Damage and the Effect of Layup in Notched Tensile Tests. Journal of Composite Materials 2005;40:1229–45.

[45] Jiang W-G, Hallett SR, Green BG, Wisnom MR. A concise interface constitutive law for analysis of delamination and splitting in composite materials and its application to scaled notched tensile specimens. International Journal for Numerical Methods in Engineering 2007;69:1982–95.

[46] Li X, Hallett SR, Wisnom MR. Predicting the effect of through-thickness compressive stress on delamination using interface elements. Composites Part A: Applied Science and Manufacturing 2008;39:218–30.

[47] Gan KW, Hallett SR, Wisnom MR. Measurement and modelling of interlaminar shear strength enhancement under moderate through-thickness compression. Composites Part A: Applied Science and Manufacturing 2013;49:18–25.

[48] Harper PW, Hallett SR. Cohesive zone length in numerical simulations of composite delamination. Engineering Fracture Mechanics 2008;75:4774–92.

[49] Livermore Software Technology Corporation. LS-DYNA keyword user's manual. Version 971 R600 2007.

[50] Davies GAO, Robinson P, Robson J, Eady D. Shear driven delamination propagation in two dimensions. Composites Part A: Applied Science and Manufacturing 1997;28:757–65.

[51] Puck A, Schürmann H. Failure analysis of FRP laminates by means of physically based phenomenological models. Composites Science and Technology 2002;62:1633–62.

[52] Reddy JN. Mechanics of Laminated Composite Plates and Shells: Theory and Analysis, Second Edition. Taylor & Francis; 2004.

[53] Buckingham E. On Physically Similar Systems; Illustrations of the Use of Dimensional Equations. Physical Review 1914;4:345–76.

[54] Suemasu H, Majima O. Multiple Delaminations and their Severity in Circular Axisymmetric Plates Subjected to Transverse Loading. Journal of Composite Materials 1996;30:441–53.

[55] Kumar S. Analysis of impact response and damage in laminated composite shell involving large deformation and material degradation. Journal of Mechanics of Materials and Structures 2008;3:1741–56.

[56] Schoeppner G a., Abrate S. Delamination threshold loads for low velocity impact on composite laminates. Composites Part A: Applied Science and Manufacturing 2000;31:903–15.

[57] Hallett SR, Green BG, Jiang W-G, Cheung KH, Wisnom MR. The open hole tensile test: a challenge for virtual testing of composites. International Journal of Fracture 2009;158:169–81.

Figures

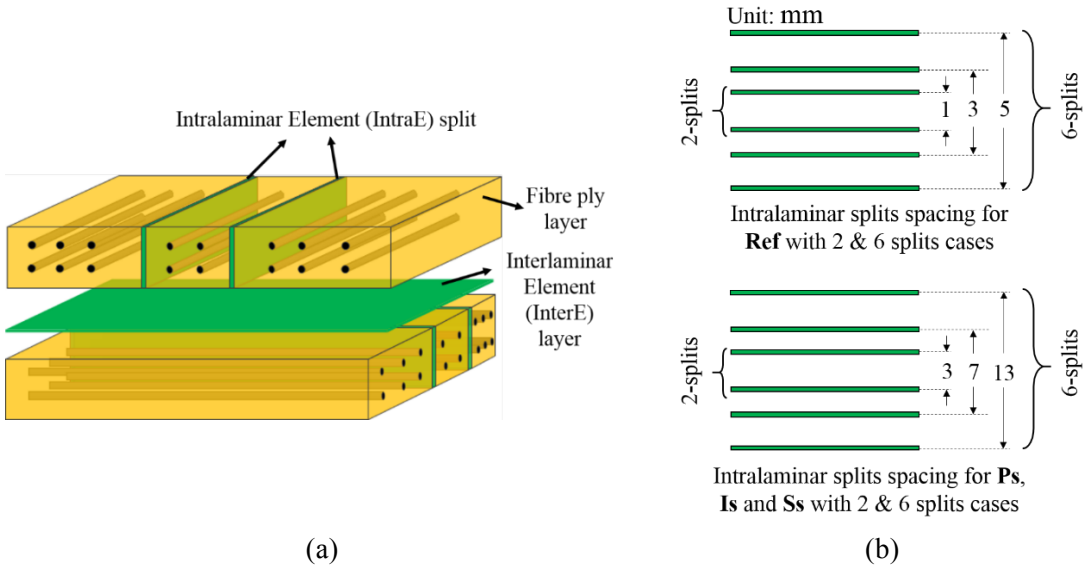

Figure 1. (a) Schematic of laminated composite plate model with the location of intralaminar elements and interlaminar cohesive elements shown in green, the two representative plies in yellow shown here is for illustration only and irrelevant to the actual models (b) Spacing dimensions of splits modelled. The middle two splits are used in 2-splits models. All six splits are used in 6-splits models.

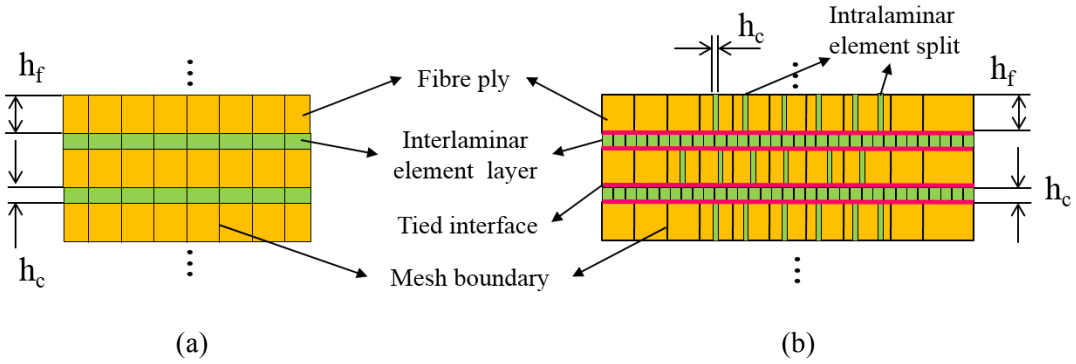

Figure 2. Cross-sectional schematics of plat models with indication of the key components and the modelling architecture. (a) Laminate models with all nodes being directed connected to each other, which are used in 0-split and 1-split model (0-split model is shown here). (b) Laminate models with tie interface that bonds non-coincident nodes, which are used in 2-splits and 6-splits model (schematic of 6-splits model is shown here for illustration).

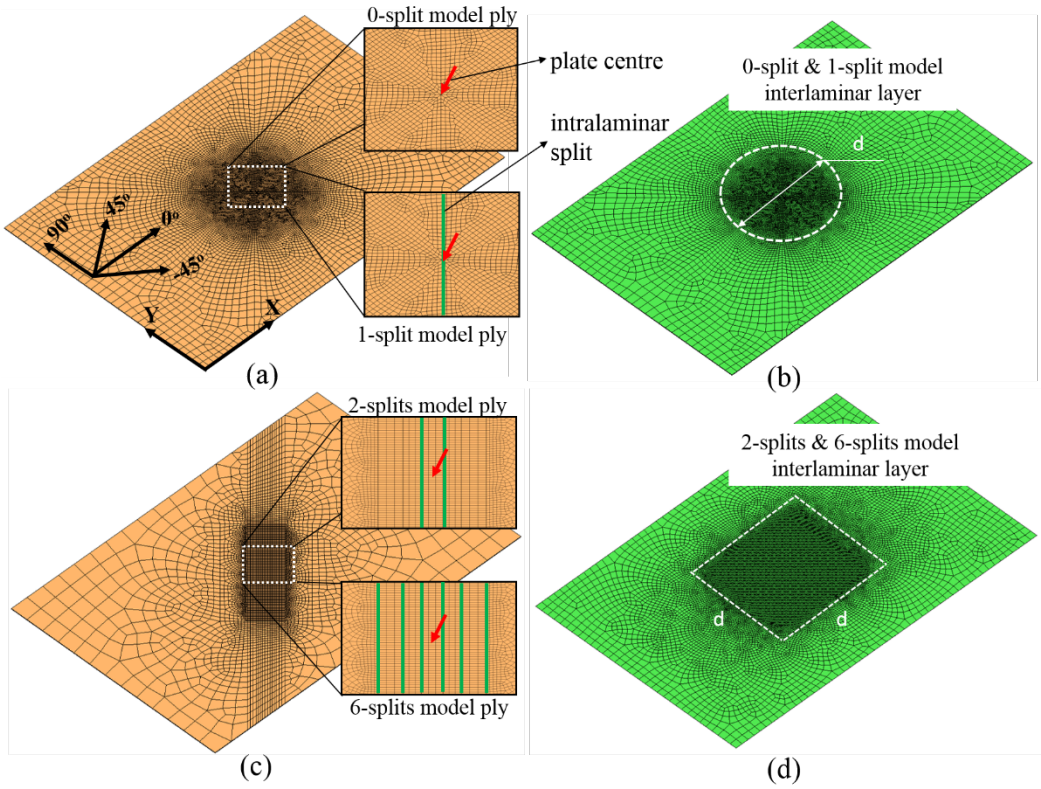

Figure 3. Mesh strategy and position of intralaminar element strips for the two types of the models. (a) The mesh scheme for the fibre ply of 0-split and 1-split models, and the position of plate centre and intralaminar element strip in 1-split model. (b) The interlaminar layers used in 0-split and 1-split models, being the same mesh as (a). (c) The mesh scheme for the fibre ply in 2-splits and 6-splits models, and the position of intralaminar element strips relative to plate centre. (d) interlaminar layer of 2-splits and 6-splits models, the mesh of these are different from (c).

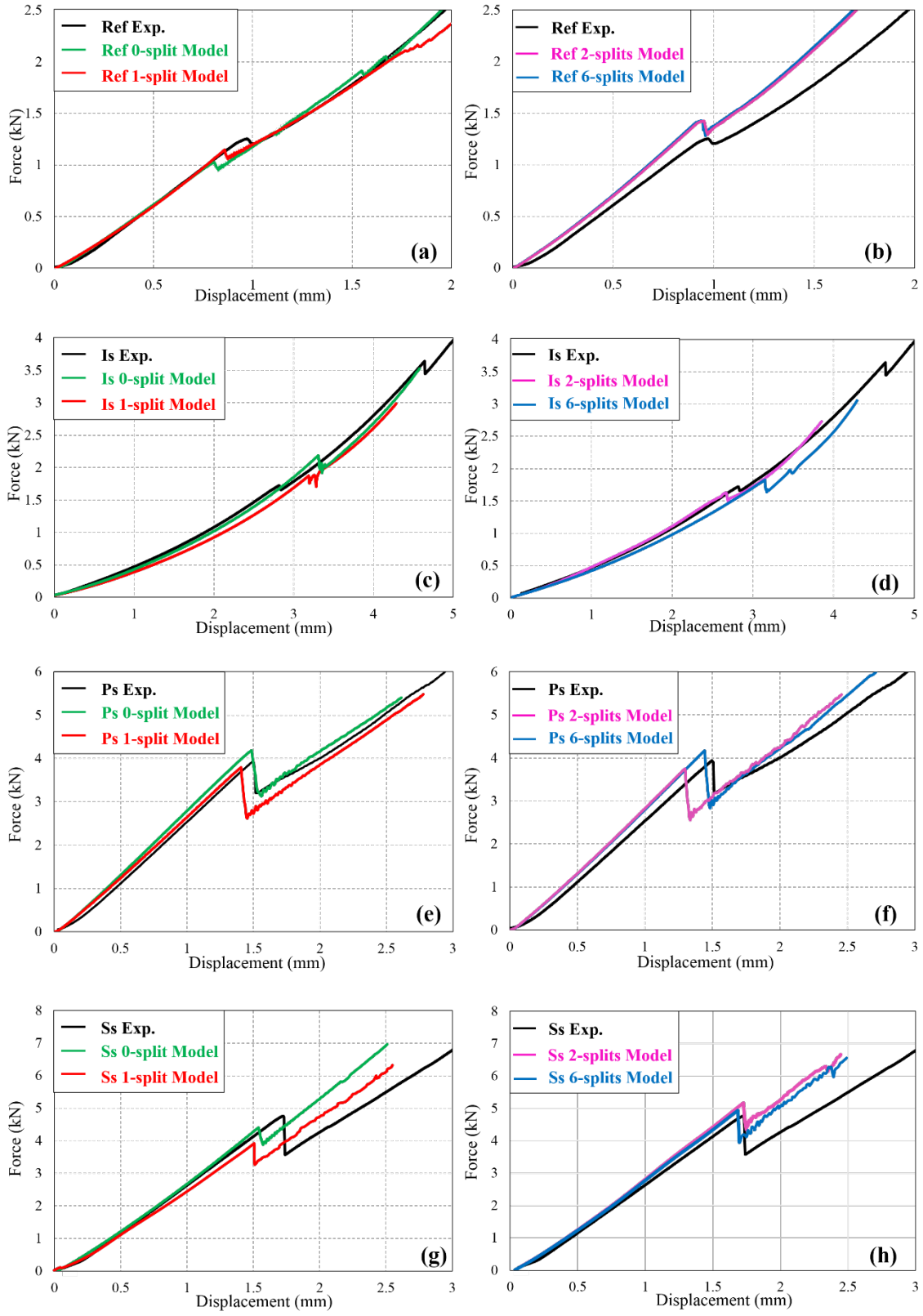

Figure 4. Comparison of load-displacement curves between all modelling approaches and experimental results of all cases [31].

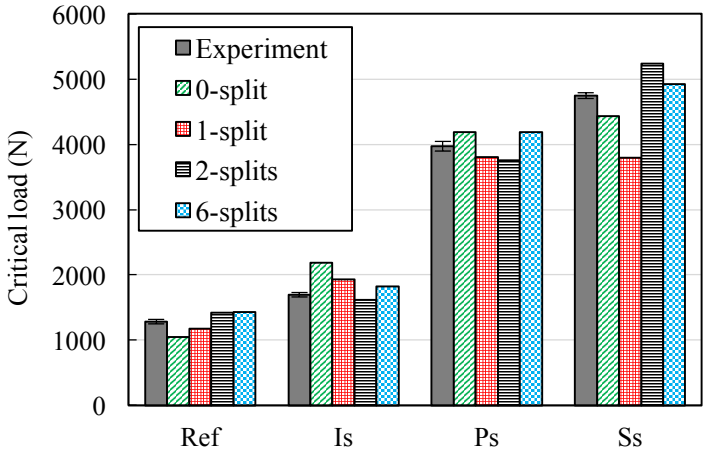

Figure 5. Comparison of load level at moment of first significant load drop (critical load) between modelling and test results.

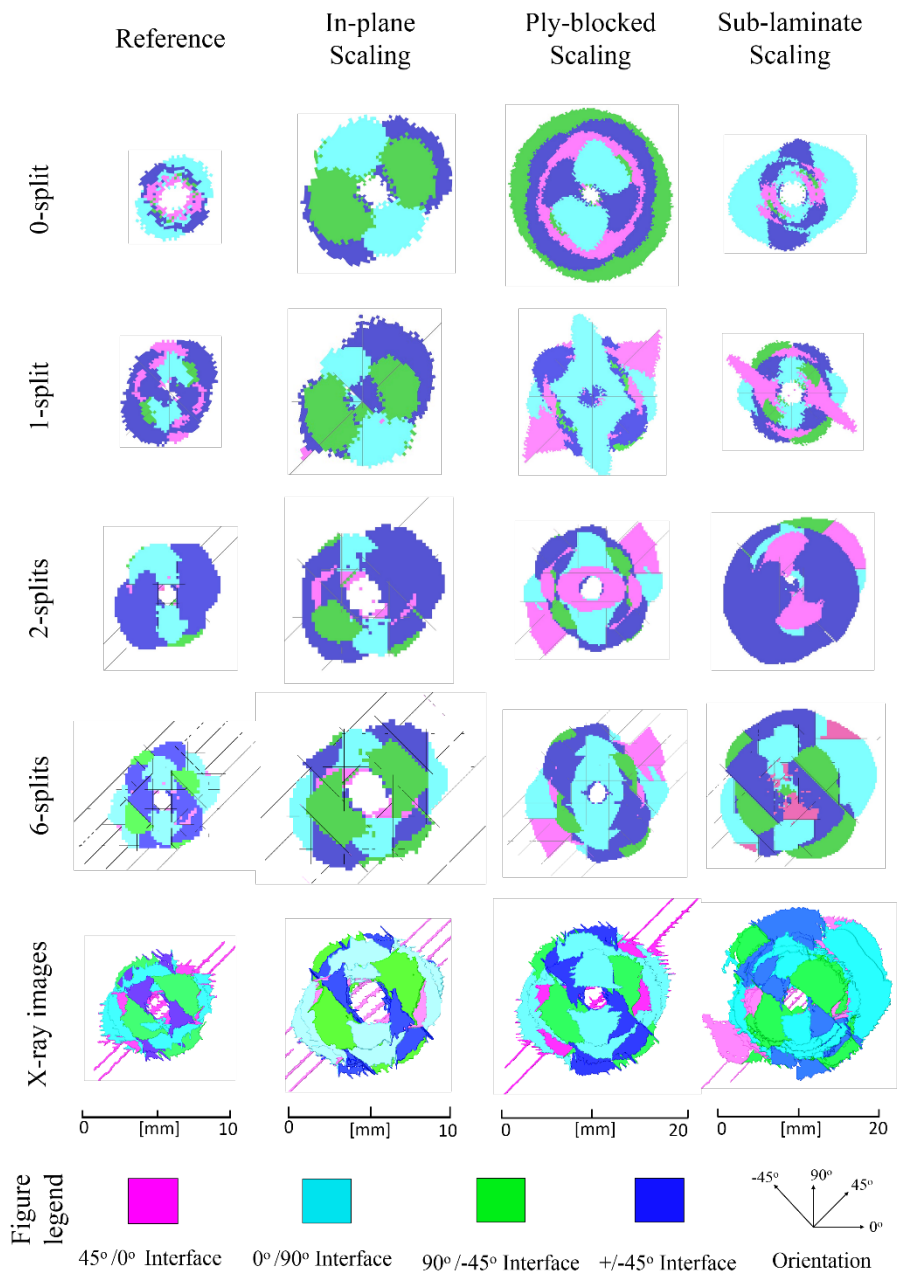

Figure 6. Comparison of projected delamination area between each FE model and X-ray images for each specimen. Colour scheme is the same as post-processed X-ray images.

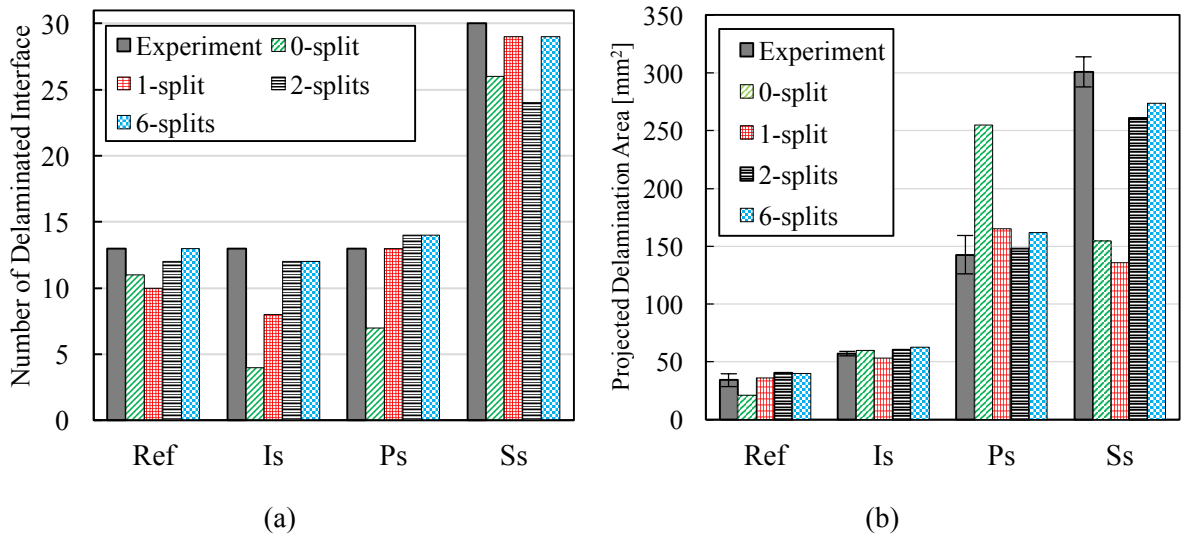

Figure 7. (a) Comparison of total number of delaminated interfaces. (b) Comparison of projected delamination area.

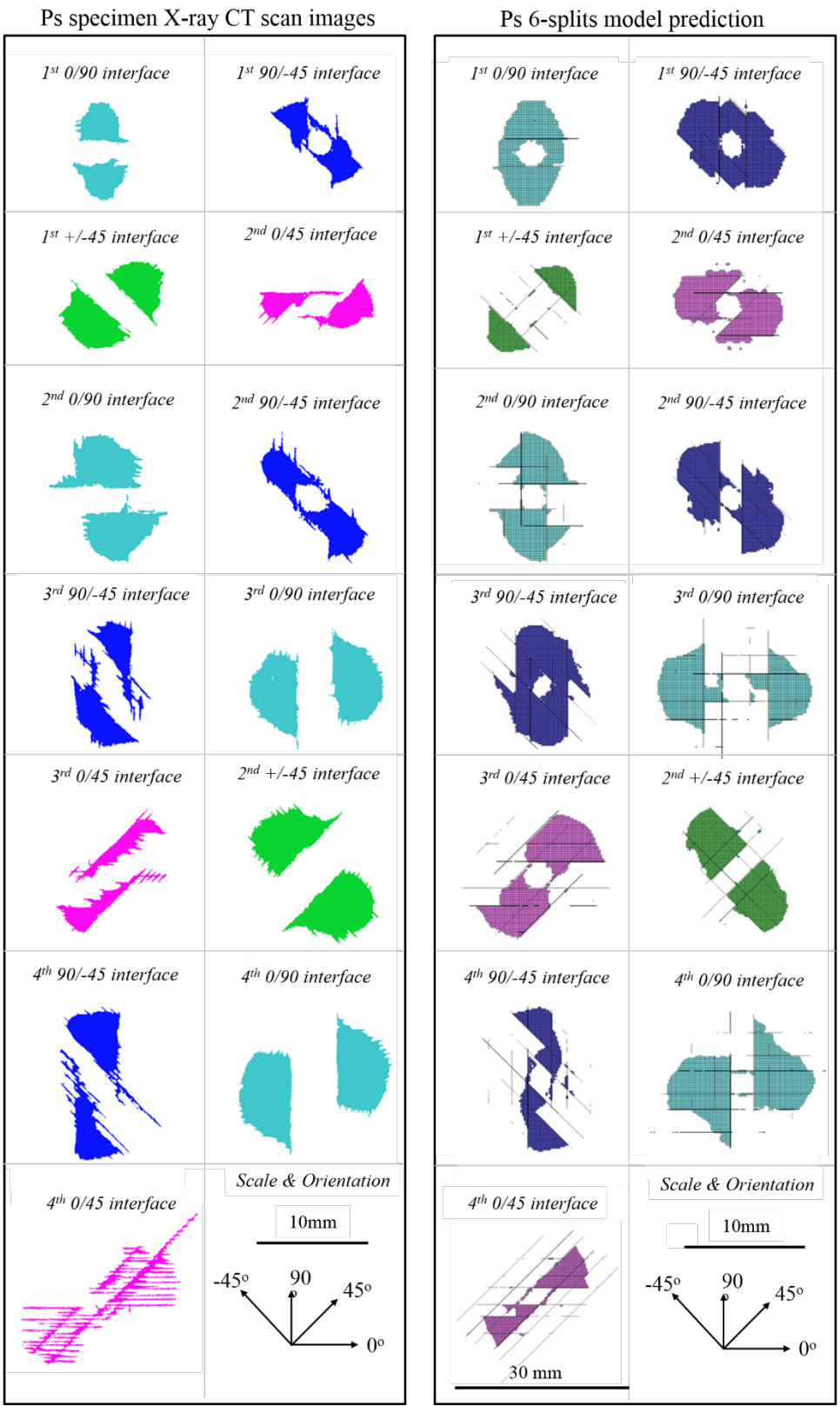

Figure 8. Individual delamination comparison between X-ray images and FE prediction of 6-splits model at each interface of Ply-block scaling (Ps) laminate; colour scheme is the same shown in above figures.[31].

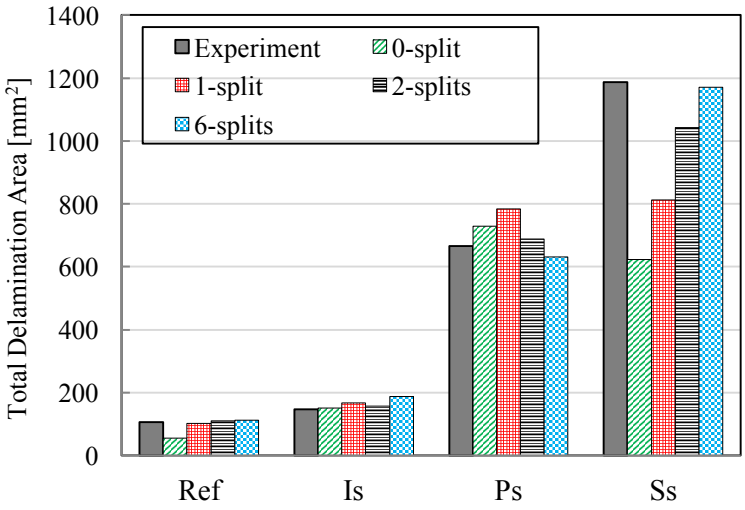

Figure 9. Total delamination area comparison between four modelling approaches and experimental results.

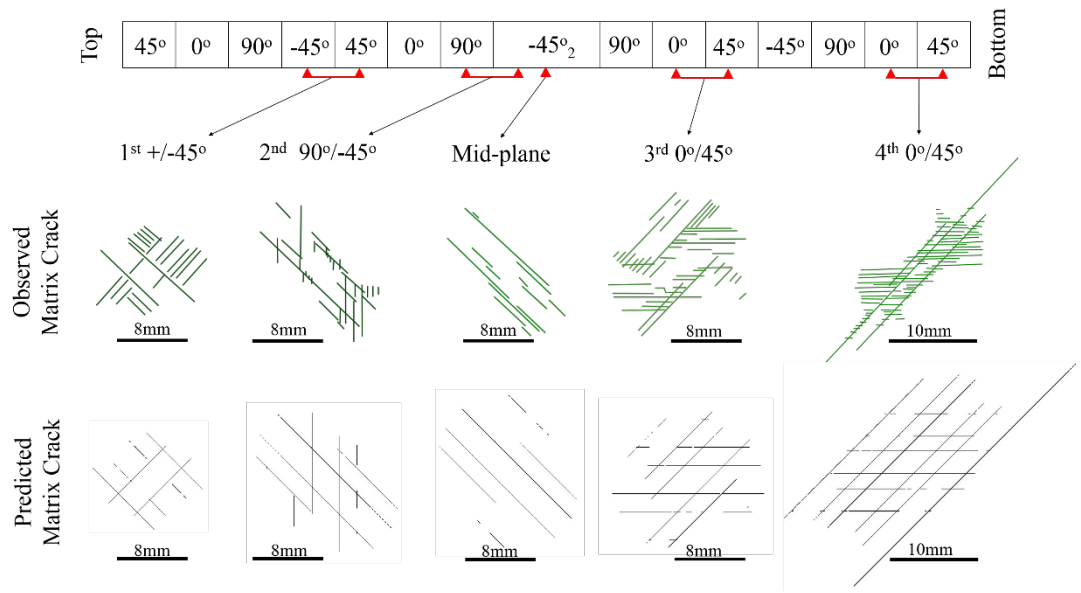

Figure 10. Comparison of characteristic matrix cracks for Ps case between numerical prediction of 6-splits model and experimental observation via X-ray images at selected locations. Stacking sequence of Ps laminate with indication of corresponding interfaces between which cracks are grouped is shown at the top of the figure.

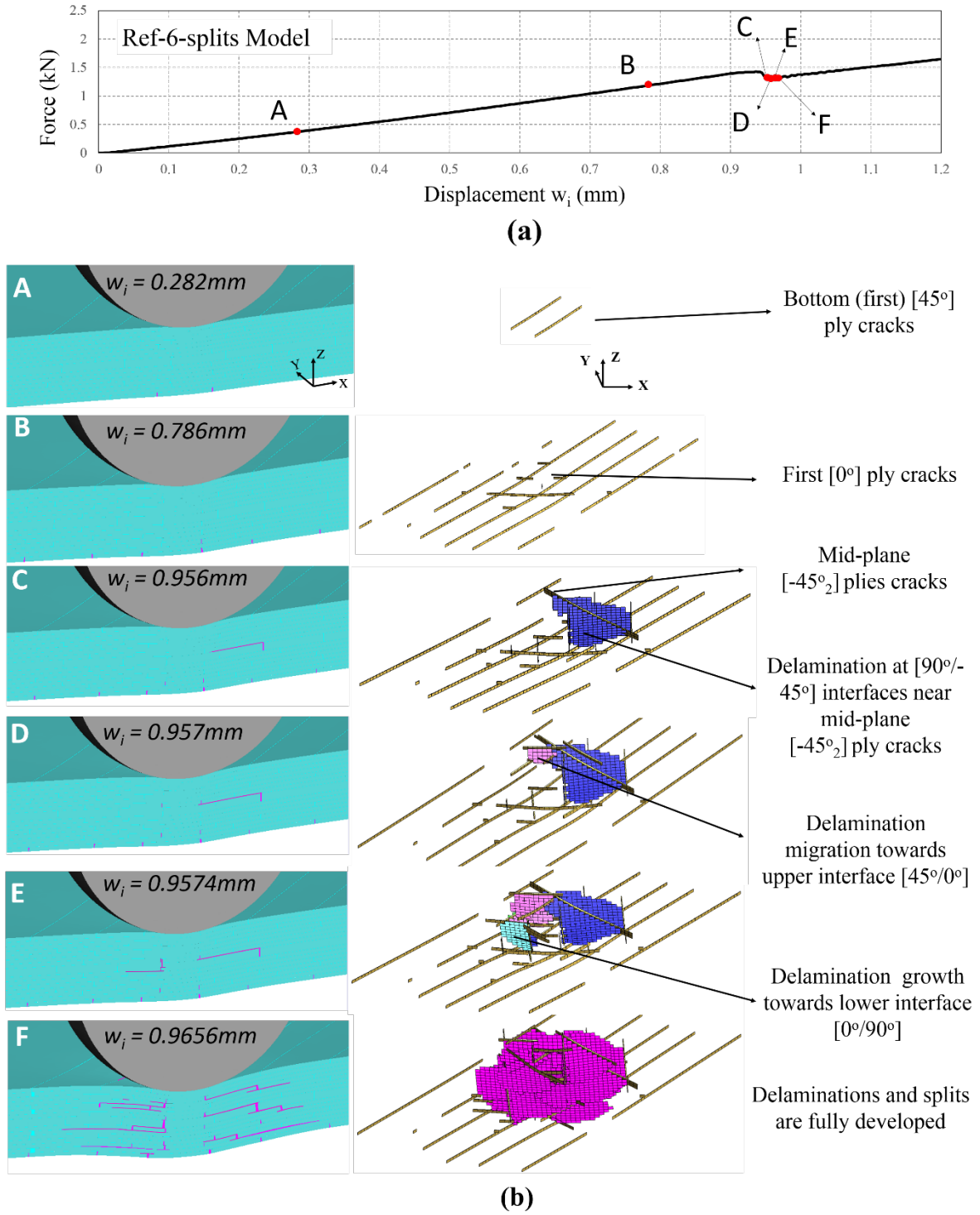

Figure 11. Predicted damage evolution attained from 6-splits model of Reference case. (a) Loading curve of Ref 6-splits model with five comparison points. (b) LHS shows the cut section view in xz plane at corresponding comparison points, elements in magenta indicate predicted inter- and intra-laminate damage; RHS shows the corresponding damage extent with predicted delamination and matrix cracks.

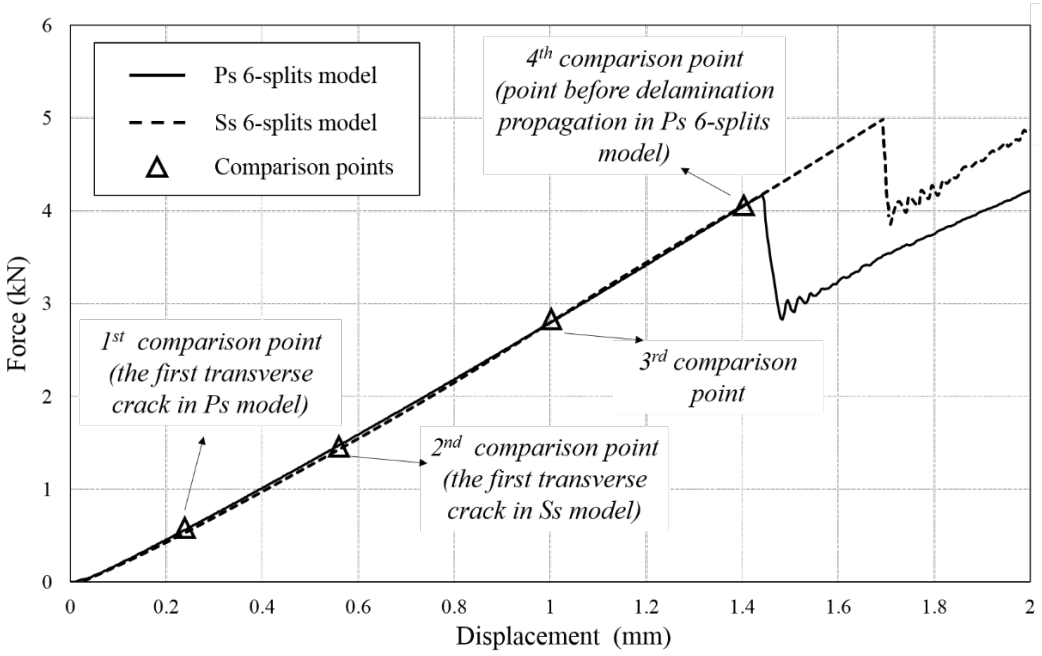

Figure 12 Load-displacement curves of Ps and Ss 6-splits model with four distinct comparison points corresponding to different indenter displacement levels.

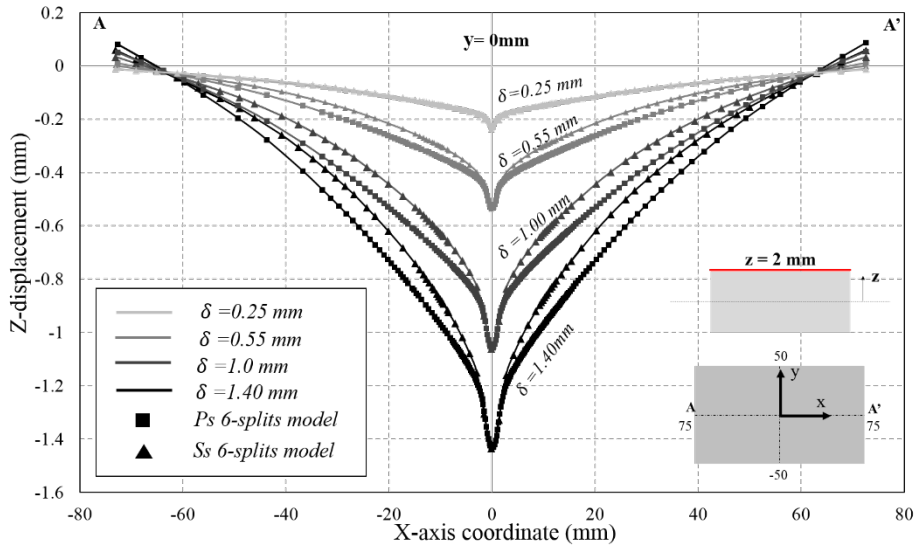

(a)

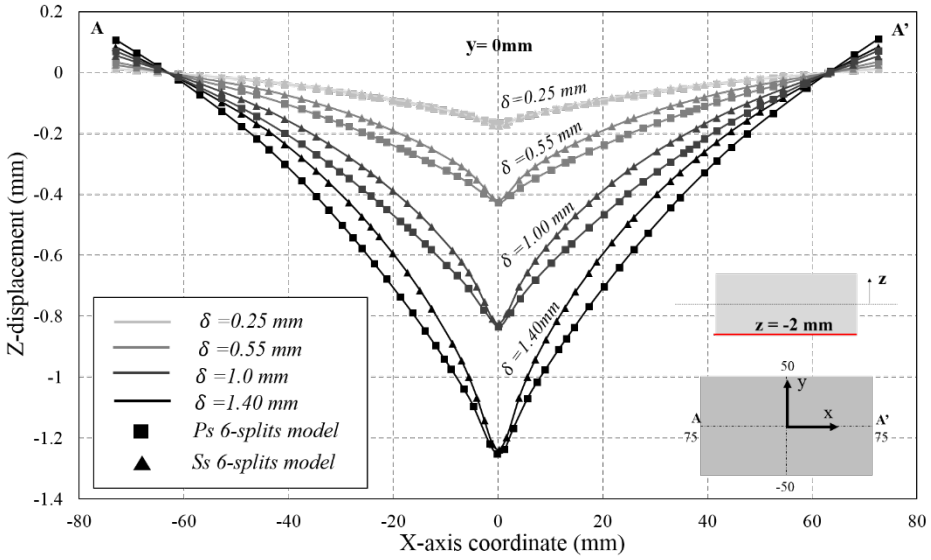

(b)

Figure 13 (a) Showing top ply central deflection profiles of Ps and Ss 6-splits model at four different comparison points defined in Figure 11. (b) Showing bottom ply central deflection profiles of Ps and Ss 6-splits model at four different comparison points defined in Figure 11.

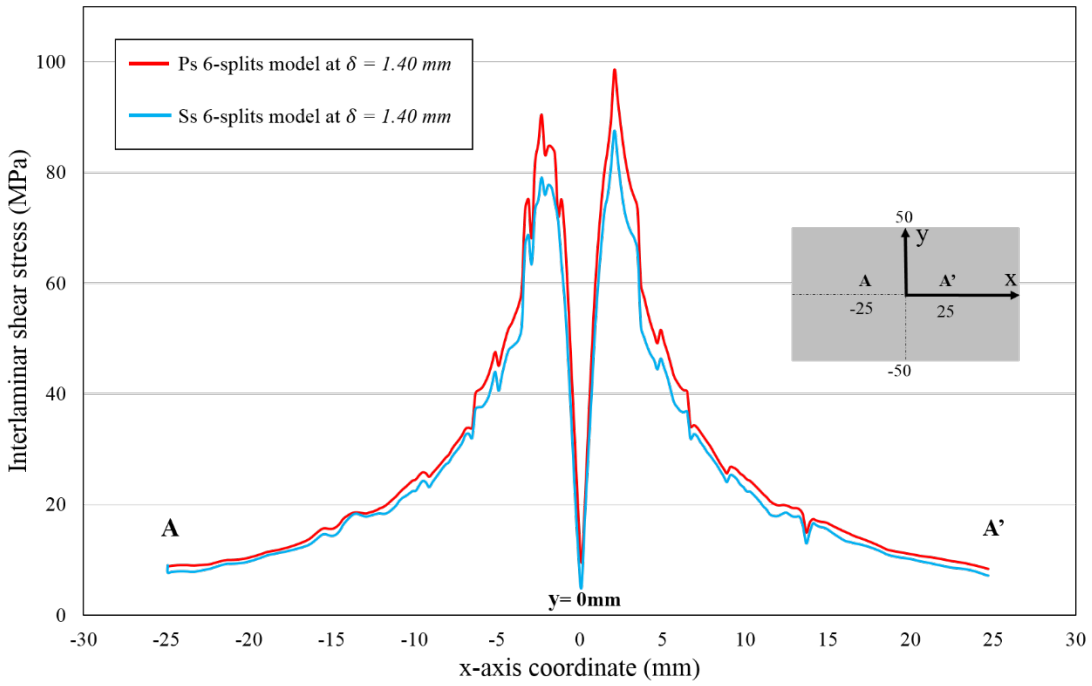

Figure 14 Interlaminar shear stress profiles at the lower mid-plane interface ([-45°/90°]) of the Ps and Ss 6-splits models.

Tables

Table 1. Characteristics of four types of specimens used in this study [31].include indenter size

Case	Lay-up	Nominal ply thickness (mm)	Overall cured thickness (mm)	In-plane Dimensions (mm)	Indenter diameter (mm)
Reference (Ref)	$[45^o/0^o/90^o/-45^o]_{2S}$	0.125	2	75 x 50	8
In-plane Scaling (Is)	$[45^o/0^o/90^o/-45^o]_{2S}$	0.125	2	150 x 100	16
Ply-block Scaling (Ps)	$[45^o_2/0^o_2/90^o_2/-45^o_2]_{2S}$	0.25	4	150 x 100	16
Sublaminate scaling (Ss)	$[45^o/0^o/90^o/-45^o]_{4S}$	0.125	4	150 x 100	16

Table 2. Material properties of IM7/8552 [32,56]**.**

ply Property	$E_{11} = 161\text{GPa}$ $E_{22} = E_{33} = 11.4\text{GPa}$ $\nu_{12} = 0.3$ $\nu_{23} = 0.436$ $G_{12} = G_{13} = 5.17\text{GPa}$ $G_{23} = 3.98\text{GPa}$ $\alpha_{11} \approx 0$ $\alpha_{22} = \alpha_{33} = 3\times10^{-5}$
Interface Property	$E_I = E_{II} = 100\text{GPa}$ $\sigma_I^* = 60\text{MPa}$ $\sigma_{II}^* = 90\text{MPa}$ $G_{IC} = 0.2\text{N/mm}$ $G_{IIC} = 0.8\text{N/mm}$; $\alpha = 1$ $\eta = 0.3$

Table 3 Comparison of critical load (F_C) obtained from experimental, analytical solution [31,50] and 6-splits numerical results.

Case	E_{eff} (GPa)	ν	G_{IIC} (N/mm)	h (mm)	F_C Exp. (kN)	F_C Theo.(kN)	F_C Num. (kN)
Ref	42.0	0.3	0.8	2	1.28	1.61	1.43
Is	42.0			2	1.70	1.61	1.83
Ps	42.0			4	3.96	4.55	4.19
Ss	51.7			4	4.73	5.05	4.92